Comparison of two-compartment exchange and continuum models of dMRI in skeletal muscle

Noel M. Naughton[1,2], John G. Georgiadis[1,2,3]

[1]Department of Mechanical Science & Engineering, University of Illinois at Urbana-Champaign, Urbana IL, USA; [2]Beckman Institute For Advanced Science and Technology, University of Illinois at Urbana-Champaign, Urbana, IL, USA; [3]Department of Biomedical Engineering, Illinois Institute of Technology, Chicago IL, USA

Abstract. Diffusion MRI (dMRI) is sensitive to micrometer spin displacements, but the image resolution is ∼mm, so the biophysical interpretation of the signal relies on establishing appropriate subvoxel tissue models. A class of two-compartment exchange models originally proposed by Kärger have been used successfully in neural tissue dMRI. Their use to interpret the signal in skeletal muscle dMRI is challenging because myocyte diameters are comparable to the rms of spin displacement and their membrane permeability is high. A continuum tissue model consisting of the Bloch-Torrey equation integrated by a hybrid lattice Boltzmann scheme is used for comparison. The validity domain of a classical two-compartment tissue model is probed by comparing with the prediction of the continuum model for a 2-D unidirectional composite continuum model of myocytes embedded in a uniform matrix, the validity domain of a classical two-component tissue model is probed. This domain is described in terms of two dimensionless parameters inspired by mass transfer phenomena, the Fourier (F) and Biot (B) numbers. The two-compartment model is valid when $B << 1$ and $F >> 1$, or when $F << 1$ and $F \cdot B << 1$. The model becomes less appropriate for muscle dMRI as the cell diameter and volume fraction increase, with the primary source of error associated with modeling diffusion in the extracellular matrix.

Keywords: two-compartment exchange; Kärger model; lattice Boltzmann method; diffusion MRI; skeletal muscle

Submitted to: *Phys. Med. Biol.*

1. Introduction

Skeletal muscle microstructure is an important indicator of muscle's functional ability, production of mechanical work. Changes in myocyte size and type, as well as in the hierarchical organization of muscle tissue have been associated with variations in functional ability (Häkkinen et al., 1998; Boonyarom and Inui, 2006; Lieber and Ward, 2013). Pertinent to the 3-D force transmission in skeletal muscle, the extracellular matrix surrounding muscle cells is thought to play a key role in force transmission from the myocyte to the tendon during muscle activation (Purslow, 2002). Current methods of determining microstructural parameters include histology, electrical impedance and dual X-ray absorptiometry, however, these methods are either highly invasive or only provide gross level information about muscle architecture. Diffusion-weighted magnetic resonance imaging (dMRI) offers an opportunity to estimate specific structural parameters of muscle microstructure in vivo, while avoiding the invasiveness of a muscle biopsy required for histological analysis (Fieremans et al., 2017; Galban et al., 2004). dMRI probes microstructure due to its sensitivity to the influence of structural barriers on self-diffusion of water. dMRI has been used to track the orientation of axons (Beaulieu, 2002) and muscle fibers (Lansdown et al., 2007) as well as provide microstructural parameter estimation for axons (Assaf et al., 2008; Nguyen et al., 2015), cancerous cells (Jiang et al., 2016), and both cardiac (Froeling et al., 2014; Mekkaoui et al., 2017) and skeletal muscle (Fieremans et al., 2017; Galban et al., 2004; Karampinos et al., 2009).

dMRI entails the use of magnetic gradients along directions chosen by the operator which sensitize the MRI signal to the random Brownian motion of the water molecules and therefore can be used to extract an apparent diffusion coefficient along the chosen direction. In muscle, the apparent diffusion coefficient changes according to the effective diffusion time (Δ_{eff}) used during acquisition. In human skeletal muscle, cells are ∼20-90 μm in diameter (Polgar et al., 1973), and are surrounded by a semi-permeable membrane (sarcolemma) which has been reported to have a significant effect on dMRI signal (Hall and Clark, 2017). The time evolution of the dMRI signal due to microstructural barriers depends on cell-scale structures due to the diffusion distance being ∼20 μm for a typical Δ_{eff} of 30 ms (Bolsterlee et al., 2017). Subcellular structures are also important (Filli et al., 2016; Scheel et al., 2013). Kinsey et al. (1999) showed that the sarcoplasmic reticulum and mitochondria have important effects on the dMRI signal in both type I and type II fibers in fish muscle. Along with these intracellular structures, changes in the extracellular space has also been shown to effect the dMRI signal. Exercise (Froeling et al., 2015), hybrid training (Sigmund et al., 2014), ischemia (Oudeman et al., 2016), weight loss (Galbán et al., 2005), and age (Porcari et al., 2018) have all been associated with changes in the extracellular structure and are reflected in the dMRI signal. These structural changes in the muscle are often associated with functional changes as well, motivating the need to understand how these changes in skeletal muscle microstructure, as measured with dMRI, affect the mechanical function of muscle. The extracellular

compartment is also associated with a longer T_2 relaxation time than the intracellular compartment, which may cause it to provide a stronger contribution to the dMRI signal, particularly for longer TE times (Heemskerk and Damon, 2007).

dMRI is a sensitive probe of the microstructure at the micrometer scale, which is the length scale of water molecule displacement during typical dMRI pulse sequence. On the other hand, dMRI has a practical voxel resolution limit of ~ 1 mm^3. All structural information below this spatial scale is "smeared" but not lost. An established method to recover microstructural information at sub-voxel levels is based on exploiting the hierarchical organization of the skeletal muscle and prior knowledge. Consistent with muscle histology and diffusion tensor imaging studies (Heemskerk and Damon, 2007; Oudeman et al., 2016; Heemskerk et al., 2010), a tissue model consisting of periodic arrays of myocytes surrounded by the endomysium matrix represents a parsimonious level of abstraction. This model is characterized by morphological (e.g. myocyte diameter, volume fraction, etc.) and physical parameters (diffusion coefficients, membrane permeability, etc.). Unlike statistical models which depend on a priori dMRI signal representations, such tissue models allow the interpretation of dMRI signal in terms of biophysical parameters which can be assessed via independent histological assays (Jelescu and Budde, 2017).

Methods of model parameter estimation from dMRI have been developed using both analytical and numerical solutions of continuous diffusion models of biological tissue. Many analytical models use a multi-compartment exchange approximation that results in a mathematical problem consisting of a set of coupled differential equations which have a closed form solution. This method was first developed by McConnell (1958), was extended to include diffusion by Kärger (1988), and has been further developed by Stanisz et al. (1997, 1998), Coatléven et al. (2014) and Haddar et al. (2016), while Karampinos et al. (2009) first applied it to muscle. This compartmental exchange method has been validated by multiple authors using Monte Carlo simulations (Szafer et al., 1995; Stanisz et al., 1997; Meier et al., 2003; Nilsson et al., 2010), as well as continuum based models Li et al. (2014). Additional authors have developed more advanced continuum based models of diffusion-weighted imaging (Hwang et al., 2003; Xu et al., 2007; Van Nguyen et al., 2014; Beltrachini et al., 2015; Hagslätt et al., 2003; Harkins et al., 2009; Russell et al., 2012). Monte Carlo models have also been developed and used to investigate how variations in skeletal muscle microstructure affect the measured signal and to improve dMRI encoding sequences in order to increase sensitivity to such variations (Lee et al., 2013; Hall and Alexander, 2009; Hall and Clark, 2017; Berry et al., 2018; Bates et al., 2017). These continuum and Monte Carlo methods are more accurate than simplified analytical models, however, they are also computationally expensive, leaving compartmental exchange models an appealing option.

Previous authors' validation of compartmental exchange models have been limited to parameter sets predominantly relevant to axons, as this was the first application area of the model (Fieremans et al., 2010; Nilsson et al., 2010; Stanisz et al., 1997; Nguyen et al., 2015), however, skeletal myocytes have larger diameters, are more densely packed,

and their membranes are more water permeable than these axons, thus presenting challenges to the compartmental exchange model's ability to correctly model dMRI in skeletal muscle. Compartment models with and without exchange have been used in the literature to estimate skeletal muscle properties (Saotome et al., 2006; Laghi et al., 2017; Karampinos et al., 2007, 2009; Jiang et al., 2016; Galbán et al., 2005; Kim et al., 2005) While previous authors have speculated on the applicability of compartmental exchange models in these regimes, namely that the model will break down, to our knowledge no one has explicitly evaluated the limits of the models' applicability in regards to interpreting dMRI data of muscle. The present work seeks to determine the applicability of the compartmental exchange model in modeling dMRI in skeletal muscle by comparing it with a hybrid-lattice Boltzmann method solution of the Bloch-Torrey equation governing the dMRI signal. Further, an attempt is made to develop general criteria for the applicability of compartment exchange models by combining the various parameters associated with the underlying diffusion physics and drawing analogies to the lumped capacitance model prevalent in mass transfer literature. Other analytical models have been proposed which interpret dMRI data while ignoring the effect of the extracellular matrix (Novikov et al., 2011; Fieremans et al., 2017), but because of the extracellular matrix's important role in force transmission, we restrict our focus to compartmental exchange models that allow the retention of this extracellular structural information.

2. Methods

2.1. Diffusion MRI in Muscle

A typical dMRI experiment involves a diffusion encoding sequence followed by an imaging sequence to form the dMRI image. The diffusion sequence involves the application of a magnetic gradient, $\boldsymbol{G}(t)$, which dephases, and subsequently rephases, the precessing hydrogen protons. After the diffusion-sensitizing gradient is applied there is a non-recoverable loss of coherence due to the diffusion of water molecules within the voxel. Ignoring the imaging sequence, the time evolution of the dMRI signal is described by the Bloch-Torrey equation (Torrey, 1956),

$$\frac{\partial \boldsymbol{M}(\boldsymbol{x},t)}{\partial t} = -i\gamma[\boldsymbol{G}(t)\cdot\boldsymbol{x}]\boldsymbol{M}(\boldsymbol{x},t) - \frac{\boldsymbol{M}(\boldsymbol{x},t)}{T_2} - \nabla\cdot(D(\boldsymbol{x})\nabla\boldsymbol{M}) \ . \qquad (1)$$

This equation describes the time evolution of the complex valued, transverse magnetic signal $\boldsymbol{M}$ under an externally applied, spatially and temporally varying magnetic field $(\boldsymbol{G}(t)\cdot\boldsymbol{x})$. Here i is the imaginary unit, γ is the gyromagnetic ratio of ^1H, $\boldsymbol{x}$ is the spin position vector, $\boldsymbol{G}(t)$ is the time-varying magnetic field gradient vector used to encode diffusion, T_2 is the spin-spin relaxation time, and $D(\boldsymbol{x})$ is the local diffusion coefficient.

A common diffusion-weighted sequence is the pulsed-gradient spin echo (PGSE) sequence proposed by Stejskal and Tanner (1965). In this sequence, shown in Figure 1a, a gradient of strength G is applied up to time $t = \delta$, turned off until time $t = \Delta$ and then

turned back on in the opposite direction (or the same direction coupled with a 180° RF pulse). This sequence is characterized by gradient timing parameters of δ and Δ, which are used to define a b-value as $b = \gamma^2 G^2 \delta^2 (\Delta - \delta/3)$. To aid in development of analytical solutions, the short gradient pulse (SGP) approximation is often employed which takes the limit of the gradient time approaching zero ($\delta \to 0$) such that the diffusion sensitizing gradient is applied at a single instant. Under this assumption, solutions to the Bloch-Torrey equation solved over simple structures are possible (Tanner and Stejskal, 1968; Szafer et al., 1995; Söderman and Jönsson, 1995), though simple structures can also be solved for more arbitrary pulse profiles (Callaghan, 1997; Codd and Callaghan, 1999), and solutions to multi-layered structures have been presented for a PGSE pulse by Grebenkov (2010). As a first approximation, diffusion is often assumed to be Gaussian which allows the dMRI signal to be modeled as

$$S = \int_V \boldsymbol{M}(\boldsymbol{x}, TE) d\boldsymbol{x}; \qquad \ln(S/S_0) = -bD^{app} , \tag{2}$$

where S is the diffusion-weighted signal integrated over the voxel, S_0 is the signal when no diffusion gradient is applied, and D^{app} is the apparent diffusion coefficient of the voxel.

Equation (2) describes the signal of unrestricted diffusion with a constant coefficient. To model the effect of complex, realistic muscle microstructure on the dMRI signal (which is not described by a simple Gaussian model), it is necessary to introduce the diffusion barriers that characterize the microstructure. Skeletal muscle structure has a hierarchical order exhibiting a long-range organization of parallel, elongated cells (myocytes) surrounded by a semi-permeable (sarcolemma) membrane and embedded in an extracellular matrix made up of collagen fibers (endomysium). This organization inspires a simplified representation of the tissue as long cylinders packed together in a hexagonal array (Figure 1b). By imposing periodic packing of the cells, a representative elementary volume (REV) can be defined. The tissue model based on this REV is defined by seven parameters: intra- and extracellular diffusion coefficients, cell diameter, volume fraction, membrane permeability and intra- and extracellular T_2 relaxation time. Both the intra- and extracellular domains contain semipermeable barriers which restrict the free diffusion of water, however, such restrictions cannot be economically modeled at the current spatial scale (micrometer). Examples of such barriers are the transverse tubular system, sarcoplasmic reticulum, mitochondria, collagen bundles in the endomysium and epimysium, capillaries, and adipocytes. Instead they are accounted for by the use of effective diffusion coefficients (D_{in} and D_{ex}) which represent the mass transport coefficients in the homogenized intracellular and extracellular compartments (Galban et al., 2004). The only diffusion barrier that is modeled directly is the myocyte membrane (sarcolemma) which is represented by a thin intercompartmental boundary with finite permeability. Unless a geometrical anisotropy is introduced in the packing of the myocytes, or by using elliptical cross-sections of the cylindrical fibers (Karampinos et al., 2009), this model corresponds to a transversely isotropic diffusion tensor. Muscle exhibits transversely (x-y plane) anisotropic diffusion (Galban et al., 2004; Karampinos

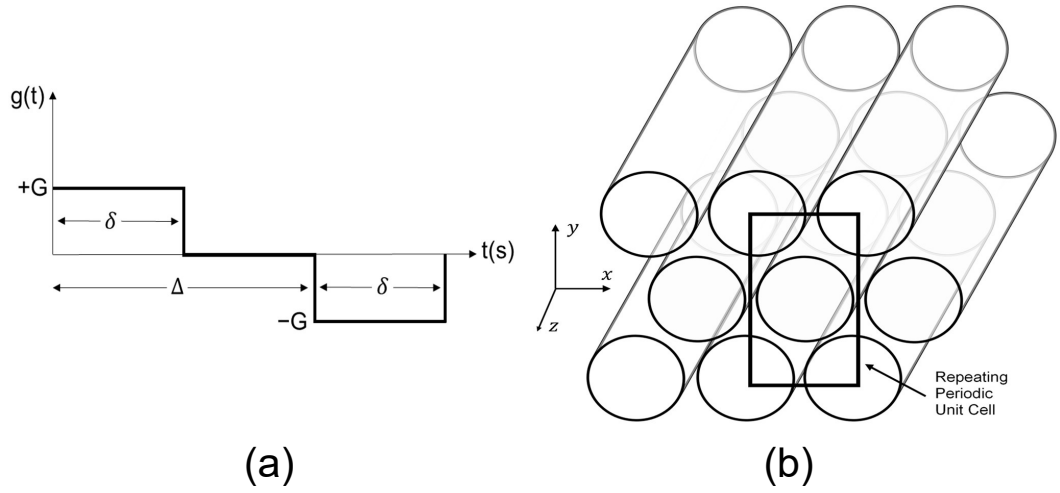

Figure 1: a) Pulsed Gradient Spin Echo (PGSE) sequence for dMRI and b) periodic muscle fiber model consisting of infinitely long cylindrical muscle fibers (intracellular compartment) bounded by an infinitesimally thin semi-permeable sarcolemma and surrounded by the endomysium (extracellular compartment). Solid rectangle designates the representative elementary volume (REV) in the x-y plane.

et al., 2009), however, the source of this anisotropy is still unresolved and outside the scope of the present study.

2.2. Numerical Model

The lattice Boltzmann method (LBM) is employed to solve the Bloch-Torrey equation (1) over the prescribed REV domain in two dimensions. LBM is a mesoscale numerical scheme that can simulate transport phenomena on regular discrete grids and has been used to solve the advection-diffusion equation (Li et al., 2013; Chen and Doolen, 1998) and the Bloch-Torrey equation (Naughton et al., submitted 2019). The key elements of the LBM scheme to integrate the Bloch-Torrey equation are provided below for completeness. Using a D2Q5 lattice stencil, the dMRI signal is given by the amplitude of the complex-valued transverse magnetization,

$$\boldsymbol{M}(\boldsymbol{x},t) = \sum_{i=0}^{4} \boldsymbol{g}_i(\boldsymbol{x},t) \ , \tag{3}$$

averaged over the REV, as implied by equation (2). The grid function $\boldsymbol{g}_i(\boldsymbol{x},t)$ is the complex spin probability distribution function representing the two components of the magnetization vector. Using the Bhatnagar-Gross-Krook model with a single relaxation time (τ), the evaluation of $\boldsymbol{g}_i$ is approximated by a diffusion step $[\boldsymbol{g}_i(t) \rightarrow \boldsymbol{g}_i'(t)]$ at each node located at $\boldsymbol{x}_i$,

$$\boldsymbol{g}_i'(\boldsymbol{x} + \boldsymbol{e}_i \cdot \delta x, t) - \boldsymbol{g}_i(\boldsymbol{x},t) = -\frac{1}{\tau}[\boldsymbol{g}_i(\boldsymbol{x},t) - \boldsymbol{g}_i^{eq}(\boldsymbol{x},t)] \ , \tag{4}$$

followed by a reaction step $[\boldsymbol{g}_i'(t) \rightarrow \boldsymbol{g}_i(t+\delta t)]$,

$$\boldsymbol{g}_i(\boldsymbol{x}, t+\delta t) = \exp\Big(-\frac{\delta t}{T_2} - i\gamma G^n \boldsymbol{x}_i \delta t \Big)\, \boldsymbol{g}_i'(\boldsymbol{x}, t) \ . \tag{5}$$

The vectors $\boldsymbol{e}_i$ $(i = 0, 1, 2, 3, 4)$ are the lattice directions for the D2Q5 stencil. The effect of spin diffusion is applied in the first step (4) by the LBM renormalization equation $D = \delta x^2(\tau - 0.5)/3\delta t$, where D is the effective diffusion coefficient at $\boldsymbol{x}_i$ and δx, δt are the grid size and time step, respectively. The effects of T_2 relaxation and forced precession from the applied magnetic gradient on the signal are included in the second step (5). This two-step scheme (4-5) constitutes an explicit first-order in time and second-order in space numerical method for the integration of the Bloch-Torrey partial differential equation. The numerical integration is performed over the REV with modified periodic boundary conditions, which include the effect of the applied gradient as first presented by Xu et al. (2007), as well as interfacial boundary conditions that allow modeling of a semi-permeable sarcolemma membrane (Naughton et al., submitted 2019).

2.3. Two-Compartment Exchange Model

The hybrid LBM scheme mentioned above has been shown to integrate the Bloch-Torrey equation accurately for the tissue model shown in Figure 1b (Naughton et al., submitted 2019). One of the aims of this study is to determine if certain existing reduced models can approximate the predictions of the LBM scheme for the dMRI signal in certain physical parameter ranges. These reduced models employ analytic solutions of simplified or limiting cases, such as the short gradient approximation or long time limit solutions. One common model is the two-compartment exchange (2CE) model introduced by Kärger (1988). The basic premises are that the MR signal in the REV can be decomposed into two components, one from the intracellular space (myocytes) and second from the extracellular space (endomysium), and the dMRI signal is homogeneous in each compartment while allowing signal exchange between compartments. Under the 2CE model, the time evolution of the intra- and extracellular compartment signal, S_{in} and S_{ex} is governed by the system of coupled differential equations

$$\frac{dS_{in}}{dt} = -4\pi^2 q^2 D_{in}^{app} S_{in} - \frac{1}{\tau_{in}} S_{in} + \frac{1}{\tau_{ex}} S_{ex} - \frac{1}{T_{2,in}} S_{in} \ , \tag{6}$$

$$\frac{dS_{ex}}{dt} = -4\pi^2 q^2 D_{ex}^{app} S_{ex} - \frac{1}{\tau_{ex}} S_{ex} + \frac{1}{\tau_{in}} S_{in} - \frac{1}{T_{2,ex}} S_{ex} \ , \tag{7}$$

where $q = \gamma|\boldsymbol{G}|\delta/2\pi$, D_{in}^{app} and D_{ex}^{app} are the apparent diffusion coefficients of the intra- and extracellular compartments respectively, τ_{in} and τ_{ex} are the mean residence times of spins in the two compartments, and $T_{2,in}$ and $T_{2,ex}$ are the T_2 relaxation times of the two compartments. The total signal attenuation in the REV can be expressed as the linear superposition of the solutions in the two compartments,

$$S(q,t) = S_{in}(q,t) + S_{ex}(q,t) \ . \tag{8}$$

This system of ordinary differential equations (6, 7) has a closed-form solution (Stanisz et al., 1998). This solution assumes uniform spin distribution at $t = 0$ which results in the initial condition

$$\frac{1}{\tau_{in}} S^0_{in} = \frac{1}{\tau_{ex}} S^0_{ex} \ , \tag{9}$$

where $S^0_{in} = \nu_{in}$ and $S^0_{ex} = \nu_{ex}$, with ν_{in} and ν_{ex} being the volume fractions of the two compartments such that $\nu_{in} + \nu_{ex} = 1$. From these relations, τ_{ex} is found to be $\tau_{ex} = (\tau_{in}\nu_{ex})/\nu_{in}$, while τ_{in} is taken from Meier et al. (2003)

$$\tau_{in} = \frac{d^2}{32 D_{in}} + \frac{d}{4\kappa} \ , \tag{10}$$

where d is the cell diameter and κ is the membrane permeability.

$D^{app}_{in,ex}$ are the apparent diffusion coefficients which represent the restriction to free diffusion caused by each compartment's geometry and are generally different from the effective diffusion coefficients of each domain in the continuum tissue model discussed above. D^{app}_{in} is defined by the analytical solution for restricted diffusion between two impermeable parallel plates and subject to the short gradient pulse (SGP) approximation. To account for the effect of finite duration diffusion gradients, an effective diffusion time (Δ_{eff}) is used in place of the diffusion time Δ. For a PGSE pulse $\Delta_{eff} = \Delta - \delta/3$; leading to the expression first presented by Tanner and Stejskal (1968)

$$D^{app}_{in} = -\frac{1}{b} \ln \left[2\frac{1-\cos(2\pi q d)}{(2\pi q d)^2} + 4(2\pi q d)^2 \sum_{n=1}^{\infty} \exp\left(-n^2\pi^2 D_{in} \frac{\Delta_{eff}}{d^2} \right) \frac{1-(-1)^n \cos(2\pi q d)}{\left((2\pi q d)^2 - (n\pi)^2 \right)^2} \right] . \tag{11}$$

Analytical expressions for the time evolution of the apparent diffusion coefficient in the extracellular space, D^{app}_{ex}, are not readily available, so a long time limiting solution is used instead. The Maxwell-Garnett model of diffusion for insulated cylinders is a low-order approximation and is accurate in the dilute packing limit ($\nu_{in} << 1$) (Sen and Basser, 2005)

$$D^{app}_{ex} = D_{ex} \left(\frac{1}{1+\nu_{in}} \right) \ . \tag{12}$$

Several extensions of the Kärger 2CE model exist but have been employed for dMRI only in axons. Coatléven et al. (2014) developed the model in a rigorous mathematical manner based on periodic homogenization techniques applied to the Bloch-Torrey equation, while Fieremans et al. (2010) also developed homogenization arguments for its domain of validity. Both formulations assume that the long-time limit solution for diffusion is valid for each compartment, resulting in $D^{app}_{in} = 0$. Because of the large size of the myocyte, this assumption is not valid in muscle tissue. To estimate the apparent diffusion coefficients, Haddar et al. (2016) presented an asymptotic model which requires the numerical solution of elliptic PDEs with source terms defined on the cell membranes. These extensions to the Kärger 2CE model are mathematically rigorous but either make assumptions that are not applicable to skeletal muscle or

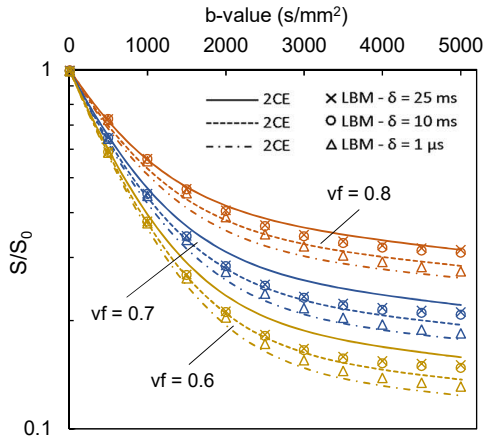

Figure 2: Comparison of continuum and 2CE models for hexagonally packed 5 μm diameter cells with varying volume fractions (vf) and gradient timing (δ). The 2CE model is solved at many more b-values than the LBM model allowing the results to be represented by a continuous curve.

require the solution of PDEs, as opposed to ODES, cf. (6-7). For this reason we retain the original phenomenological formulation of the Kärger model. The chosen apparent diffusion coefficients (11-12) allow the parameterization of the 2CE model in terms of intrinsic (biophysical) and extrinsic (dMRI sequence) parameters of the tissue model without additional computational cost, particularly for characterizing the extracellular domain (Haddar et al., 2016; Nilsson et al., 2010).

3. Results

Previous authors have shown good agreement between various formulations of two-compartment exchange (2CE) models and Monte Carlo (Fieremans et al., 2010; Nilsson et al., 2010; Stanisz et al., 1997) or Finite Element (Li et al., 2014) simulations of restricted diffusion in cell diameters smaller than 15 μm and volume fractions less than 0.70, which relates to typical values for axons. Myocytes are much larger (up to 90 μm) and are packed more densely (reaching volume fractions up to 0.95), so it stands to reason that the validity of the homogenization assumption made in the 2CE model needs to be revisited for muscle. Simulations were performed for a range of 2CE model parameters, extending the microstructural regime from axons to myocytes. Systematic variation of model parameters and comparison with the continuum LBM model allows the delineation of the region of applicability of the 2CE model. For the continuum model, spatial and temporal discretizations were chosen according to the cell diameter and are given in the supplementary information.

The 2CE model makes use of the SGP approximation, however, this approximation is often not valid for dMRI sequences employed in clinical settings due to hardware constraints and safety considerations. To investigate how the 2CE model behaves in cases where the SGP approximation is violated, simulations with the continuum model

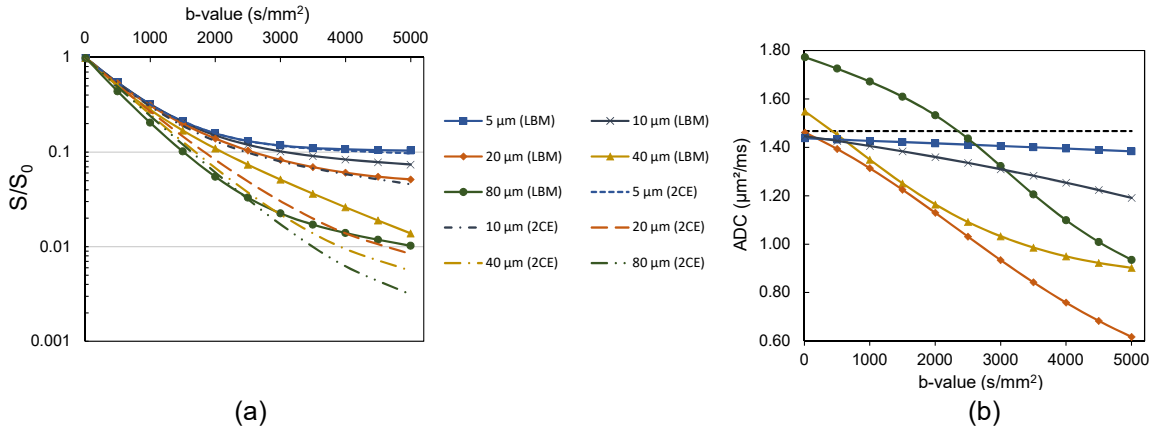

Figure 3: a) Comparison of continuum and 2CE models for hexagonally packed disks of increasing diameter and volume fraction of 0.5, and b) comparison of extracellular ADC from the LBM scheme with the 2CE model (black dashed line). PGSE timing parameters were TE/Δ/δ = 100/50/10 ms.

were performed for a cell diameter of 5 μm and the following dMRI PGSE sequence parameters: diffusion time (Δ) of 50 ms, TE of 100 ms and three different gradient durations (δ) of 1 μs, 10 ms and 25 ms, for b-values of 0 to 5000 s/mm^2 (Figure 2). The remaining biophysical parameters were chosen to lie within the range of published values available in skeletal muscle literature. The intra- and extracellular diffusion coefficients were 1.4 and 2.2 respectively $\mu m^2/ms$ (Seland et al., 2005; Helmer et al., 2006; Åslund and Topgaard, 2009; Ababneh et al., 2005; Silva et al., 2002; Morvan, 1995; Saab et al., 1999; Babsky et al., 2008), and T_2 values were 32 ms for the intracellular domain and 100 ms for the extracellular domain (Seland et al., 2005; Saab et al., 1999). Unless otherwise noted, these values are used for all subsequent results. Impermeable cell boundaries were first assumed in order to allow direct comparison of the intra- and extracellular signals between the two models. When the SPG approximation is satisfied ($\delta = 1\mu s << \Delta$), there is agreement between the two models, particularly for the smaller intracellular volume fractions. For a larger volume fraction (vf = 0.80), the 2CE model overestimates the signal attenuation compared with the LBM scheme. In all cases pertaining to the small diameter cells, there is general agreement between the two models, suggesting that the 2CE model behaves correctly, at least in terms of trends, even when $\delta << \Delta$ is not strictly satisfied, though progressively larger violation of the assumption will lead to larger inaccuracies (Li et al., 2014). As the gradient duration (δ) increases, the 2CE model begins to progressively underestimate the signal attenuation. The 2CE model appears to perform well for small (5 μm) diameter cells, but muscle cells are typically much larger.

Figure 3a shows how the models compare for increasing cell diameter and a fixed volume fraction of 0.50. Again, the best agreement between the models occurs at the smaller cell diameters. Figure 3b shows the apparent diffusion coefficients (ADC) defined

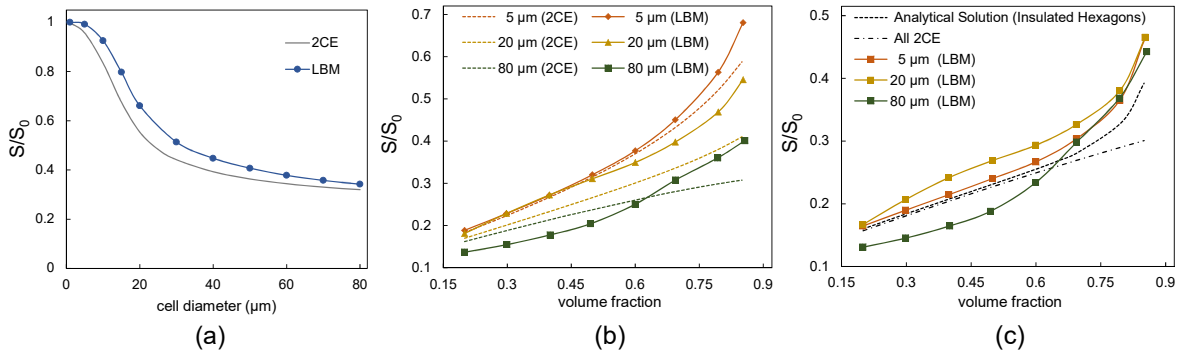

Figure 4: a) Comparison of intracellular signal vs cell diameter, b) total signal vs volume fraction for multiple cell diameters, and c) extracellular signal vs volume fraction for multiple cell diameters.

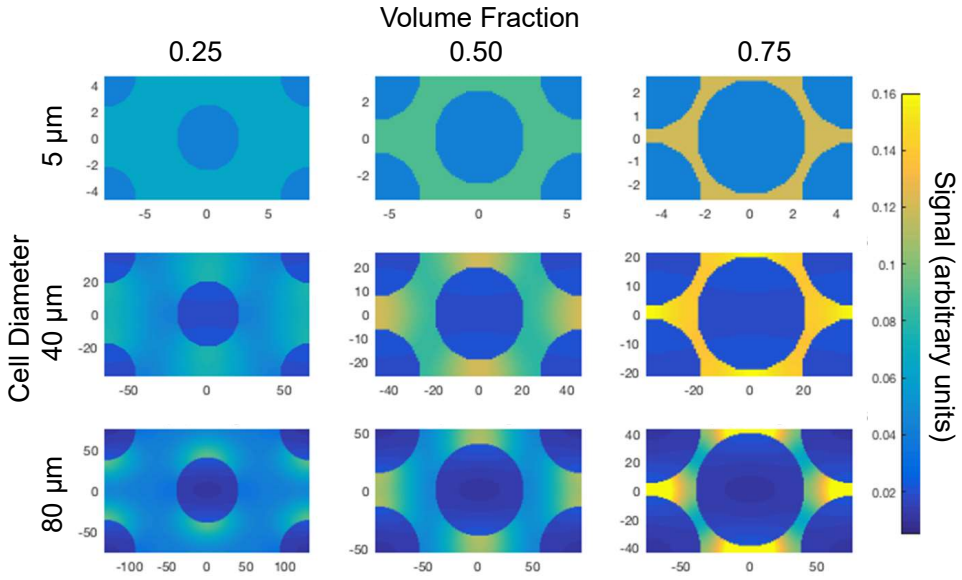

Figure 5: Local signal fieldmaps for cell diameters of 5, 40 and 80 μm (top to bottom) and volume fractions of 0.25, 0.50 and 0.75 (left to right).

over only the extracellular space; recall that in these simulations the cell boundaries are assumed to be impermeable. Because the 2CE model is based on a long-time limit solution, it exhibits no sensitivity to cell diameter or b-value while the LBM solution clearly exhibits sensitivity to both.

As Figure 3 indicates, the accuracy of the 2CE model degrades as the b-value increases. However, it is practical to limit our model comparison to clinically-relevant pulse sequence parameters and investigate how changes in physiological parameters affect the signal. Clinical dMRI acquisitions routinely involve only one b-value, so a single PGSE pulse is employed with b-value = 1000 s/mm^2 and timing parameters: TE = 100 ms, Δ = 50 ms, δ = 10 ms. The results, shown in Figure 2, suggest that the intracellular volume fraction strongly affects the accuracy of the 2CE model. In order to

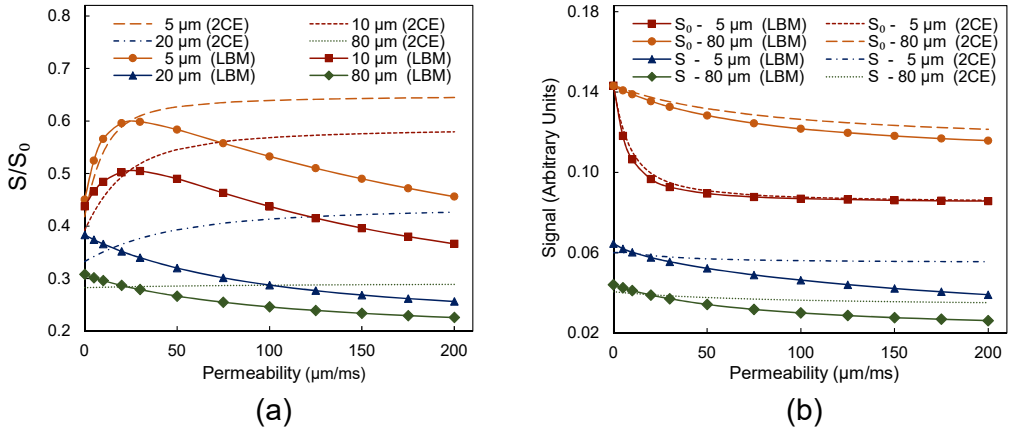

Figure 6: a) Comparison of the two models for changes in permeability for different cell sizes and a volume fraction of 0.7. b) Comparison of the S and S_0 signals separately. There is good agreement between the two models for the S_0 signal while the S signal shows increased attenuation in the LBM scheme as the permeability increases. It is the ratio of the S and S_0 signals in the LBM solution that produces the change of slope in (a) while the lack of signal attenuation in the 2CE model results in the absence of slope change.

further explore this behavior, simulations for multiple volume fractions were performed. In Figure 4a the intracellular signal is plotted for increasing cell sizes; since the cells are impermeable, this signal is insensitive to volume fraction. In Figure 4b the total intra- and extracellular signals are compared for various cell sizes, and in Figure 4c only the extracellular signal is compared over a range of volume fractions. The Maxwell-Garnett diffusion approximation used in the 2CE model does not depend on cell size so only one extracellular result exists for all cell sizes. Additionally, the analytical solution given by Perrins et al. (1979) at the long-time limit for insulated disks in hexagonal packing is shown. This analytical solution is the most accurate limiting solution possible for the considered REV because it matches the prescribed geometry. The validity of the two-compartment exchange model depends on the degree of spatial homogeneity in the signal within each compartment. This homogeneity is important in modeling the effect of intercompartment exchange, as well as justifying the long-time limit approximations in solving the diffusion problem. A direct method to determine the degree of homogeneity is to examine a fieldmap of the signal given by the results to the LBM scheme. Fieldmaps for a combination of three volume fractions and three cell diameters are shown in Figure 5.

Simulations up to this point have considered impermeable boundaries in order to compare the signal in the intra- and extracellular compartments separately, however, this consideration needs to be relaxed. Muscle cells are surrounded by a semi-permeable membrane (sarcolemma), which facilitates exchange between the cell interior and the surrounding extracellular compartment. There is no consensus value for the permeability of the sarcolemma but reported values range from 13 $\mu m/s$ (Landis et al., 1999) to 400

$\mu m/s$ (Tanner, 1978), with the upper range generally considered to be an overestimate (Fieremans et al., 2017). A comparison of the 2CE and LBM model predictions was made for different values of sarcolemma permeability in the range of 0 - 200 $\mu m/s$, and the results are shown in Figure 6 for a volume fraction of 0.70.

4. Discussion

The continuum problem formulated in Section 2.2 constitutes a forward problem: the geometry and parameters of the composite tissue model are specified and the evolution of the signal is computed. The LBM scheme provides an accurate numerical solution to the forward continuum problem described by the Bloch-Torrey equation, while the two-compartment exchange (2CE) model provides an approximate solution subject to a number of limiting assumptions. As such, we consider the continuum LBM solution the standard against which the validity of the 2CE model can be determined. The advantage of general two-compartment models is that they consist of ordinary differential equations, which allows for substantially faster solution of the forward problem than the continuum model. This is important because many simulations are typically required to solve the inverse problem of dMRI, which involves extracting parameters from the measured signal. However, this speed advantage has to be assessed in light of the model accuracy. Several authors have used two-compartment (Kim et al., 2005; Galbán et al., 2005) and two-compartment exchange (Karampinos et al., 2009; Laghi et al., 2017) models to interpret dMRI measurements in skeletal muscle, so we take the opportunity here to assess the accuracy of these models when applied to a parsimonious tissue model. Some of these attempts have limited their interpretation of dMRI signal only to the estimations of apparent diffusion coefficients. However, correct estimation of microstructural features of skeletal muscle, in particular pertaining to the extracellular matrix which surrounds skeletal muscle, is important in analyzing the transmission of force generated during muscle contraction (Purslow, 2002). This motivates the use of biophysical tissue models which preserve important features of the microstructure, such as the histoarchitecture of the extracellular matrix (endomysium). Skeletal muscle cross-sections reveal irregular, convex polygonal myocytes surrounded by a contiguous endomysium matrix. Models which explicitly consider such structural features (such as the 2CE model) ultimately must account for this disorder, however, in order to provide confidence in their ability to represent changes in the underlying microstructure, it is necessary to first compare them to more ordered structural systems such as the REV considered here.

2CE models are based on a number of limiting assumptions about the tissue structure which have been shown to be appropriate in modeling diffusion in axons (Fieremans et al., 2010; Nilsson et al., 2010; Stanisz et al., 1997; Nguyen et al., 2015), but skeletal muscle has structural characteristics which are not consistent with these assumptions. Several authors have commented on the limits of these assumptions, however, to the best of our knowledge, no one has systematically investigated the

accuracy of two-compartment models when applied to skeletal muscle. We began our investigation by modeling tissue in a regime where two-compartment models are known to be accurate (small diameter cells subject to the SPG approximation), and then extended microstructural parameters one at a time to encompass typical values of muscle dMRI (gradient duration, diameter, volume fraction, and permeability). By comparing with the continuum numerical solution, the accuracy of the 2CE model for muscle can be addressed, its weaknesses evaluated, and suggestions made for further improvements. While the ultimate goal of such models is to use them in an inversion process capable of determining microstructural parameters based on measured dMRI signal, a prerequisite for accurate inversion is the ability to correctly characterize the forward problem of how microstructural parameter changes relate to changes in the dMRI signal. Therefore, we restricted our analysis to how the 2CE represents the underlying physics and did not consider its usefulness in the inversion processes of fitting the model to dMRI measurements.

Figure 2 demonstrates two advantages of the 2CE model. First, the results underline the effectiveness of the SGP approximation in modeling the intracellular signal. This approximation involves the adjustment of the signal decay by defining an effective diffusion time, Δ_{eff}, to account for limited finite gradient times. For small gradient timings δ, the 2CE model overestimates the signal attenuation, but as δ increases, this trend is reversed. While it appears that the model is most accurate for δ=10 ms, this is coincidental. The effect of increasing δ causes the 2CE model to progressively underestimate signal attenuation, and this value happens to correspond to the point where the initial overestimate of the model for small δ and the gradual underestimation from increasing δ cancels out. For all gradient timings there is general agreement between the two models, particularly for b-values $< 1000\ s/mm^2$, suggesting that for small cell diameters, the violation of the short gradient pulse approximation, up to the extent studied, does not affect the validity of the 2CE model. Li et al. (2014) examined the case when $\delta = \Delta$ and found that the SGP approximation was not appropriate in such a case, however, for moderate violation as examined here ($\delta = \Delta/2$), the SGP approximation appears to still be sufficient. The second advantage of the 2CE model is the ability of the extracellular signal to account for changes in the intracellular volume faction at low volume fractions. It is known that the Maxwell-Garnett approximation breaks down as the volume fraction increases, which is consistent with the increasing disagreement between the models for the larger volume fraction.

Healthy skeletal muscle consists of large diameter (20-90 μm) cells, although atrophied myocytes can be smaller. For 5 μm cell diameters, Figure 3a shows agreement between the continuum and two-compartment model predictions over a wide range of b-values. The sensitivity of dMRI diffusion displacements (and ability to resolve smaller spatial scales) increases with b-value. As the cell diameter increases, the error in the 2CE model increases and this can be attributed to inaccuracies in modeling the extracellular signal. Figure 3b indicates that there is little variation in the signal as b-value increases for small cell diameters, so the assumption that the extracellular signal is represented by

the long-time limit is valid. However, as the cell diameter increases for a fixed volume fraction, so does the size of the extracellular domain. Larger extracellular domains means that the diffusing spins will explore less of the extracellular space for a particular Δ, thus leading to stronger spatial gradients in the extracellular domain (Figure 5). These gradients are not associated with a mono-exponential decay of the extracellular signal and this behavior is not approximated by the long time limit solution; the long-time limit solution is not affected by changes in cell diameter or b-value (Sen and Basser, 2005).

Healthy skeletal muscle cells are densely packed with volume fractions up to 0.95, so the results of Figure 3 for a volume fraction of 0.50 need to be extended. Figure 4 shows the joint effect of cell diameter and volume fraction on the different components of the dMRI signal. For low volume fractions and small cell diameters, there is good agreement between the two models and this can be attributed to the fact that the Maxwell-Garnett approximation is more accurate at smaller volume fractions, and smaller cell diameters allow for the long-time limit state to be reached earlier. The effect of volume fraction is demonstrated in Figure 4c which shows how the error in the extracellular signal for the 2CE model increases with volume fraction. The continuum model results converge and agree (in trend) with the analytical long-time solution developed by Perrins et al. (1979), rather than the 2CE model. However, the analytical solution is unique to the periodic hexagonal packing employed in the LBM simulations and is not representative of other packing arrangements. Others (Nguyen et al., 2015; Nilsson et al., 2010) have found that the 2CE model is well suited for estimating volume fraction by solving the inverse problem, however, their investigations were limited to volume fractions below 0.70 where the 2CE model agrees with the LBM solution.

The interaction between the effects of cell diameter and volume fraction on the applicability of the long time limit approximation is illustrated in Figure 5. For small diameters (5 μm) the extracellular signal is homogeneous, suggesting that the long time limit is regime is achieved. As the cell size increases and when the volume fraction creates an extracellular topology such that the distance between diffusion barriers (in this case sarcolemma membranes) is larger than the diffusion distance ($\sim\sqrt{D\Delta}$), signal gradients within the domain appear, thus weakening the homogeneous signal assumption of the 2CE model. The existence of such gradients helps explain the trends shown in Figures 3 and 4, where larger cell diameters and volume fractions are associated with larger discrepancies between the 2CE and continuum LBM models. On the other hand, as the volume fraction increases, the extracellular length scale decreases, leading to better approximation by the long time limit. This is in agreement with the results of Meier et al. (2003), and with Figure 4c which shows that the LBM scheme's predictions of the extracellular signal for all cell diameters converge as the volume fraction increases. The numerical solutions approach the analytical solution of Perrins et al. (1979), suggesting that sufficiently dense-packed configurations satisfy the long time limit approximation. This is most clearly seen in Figure 5 for a 40 μm diameter cell. The extracellular signal distribution contains spatial gradients for a volume fraction of 0.50, but these

gradients are reduced and the domain becomes more homogeneous as the extracellular space becomes more restricted when the volume fraction is increased to 0.75.

Creating signal gradients in each compartment also affects the spin exchange between the compartments. Intercompartmental exchange in the LBM scheme is related to the signal difference across the membrane interface (Naughton et al., submitted 2019), and not the average compartment values, as per the 2CE model. Decreasing the membrane permeability increases these interfacial differences, thus exacerbating the discrepancies between the two models. For small cell sizes and as the permeability increases, Figure 6a shows that the 2CE model remains accurate for permeability values up to $\sim$30 $\mu m/$s, but beyond this value, the two models diverge. For larger cell sizes, the agreement is poor for all permeabilities due to other, already discussed, inaccuracies in the 2CE model. Figure 6b shows that this disagreement is mostly the result of failure in modeling the diffusion-weighted signal. While the S_0 signals are in good agreement, the signal (S) predicted by the 2CE model does not exhibit the same amount of attenuation as seen in the LBM model for increasing permeability. This suggests that the deficiency of the 2CE model does not come from the intercompartmental exchange term per se, as it would also manifest itself in the case where no diffusion gradient is applied. There is some disagreement in the predicted S_0 signals for 80 μm diameter cells suggesting that as the compartment size increases, spatial gradients develop at the membrane interface due to the different compartment T_2 values. However, the poor accuracy of the diffusion-weighted signal implies that the inaccuracy of the 2CE model is mostly due to the diffusion-weighted terms in the 2CE model. The contribution of finite permeability cannot be estimated by the effective diffusion coefficients of the two compartments under the assumption that they are separated by an impermeable wall (as assumed by the 2CE model). The observed change in slope of the LBM solution for 5 and 10 μm diameter cells in Figure 6a for increasing permeability is a result of the difference in T_2 for the intracellular and extracellular compartments. The 'hump' is a manifestation of a much smaller $T_{2,in}$ (32 ms) than $T_{2,ex}$ (100 ms). If the T_2 values are equal, or if $T_{2,ex}$ is smaller than $T_{2,in}$, there is instead a monotonic decrease of the signal ratio with increasing permeability (results not shown). This behavior has also been observed by Harkins et al. (2009). These results suggest that while two-compartment (and Kärger) models are accurate for small diameter cells that are not tightly packed, they are not sufficient for large diameter, tightly packed cells. Consequently, the indiscriminate approach of using the general 2CE model as formulated for solving the inverse problem from muscle dMRI signal is not justified. Instead, we propose a more nuanced approach involving the examination of the parameter domain where 2CE is accurate.

Previous authors have discussed the limits of the two-compartment exchange model; it is useful to briefly revisit some of their points and expand upon them in light of more recent results. Spatial signal homogeneity within each compartment is a key qualitative premise of the compartmental exchange model. We propose using key characteristic length and time scales to delineate the domain of applicability of the homogeneity assumption. Stanisz et al. (1997) describes the three relevant length scales associated

with the PGSE pulse: the diffusion length ($l_d = \sqrt{Dt_d}$), the restriction length (l_r, typically the cell diameter) and the de-phasing length ($l_g = D/\gamma G$). Disparities between these length scales define different domains of signal behavior. For example, the Kärger model typically assumes $l_d >> l_r$ which is necessary for the compartmental diffusion to be Gaussian. Relevant time scales in the present problem are the diffusion time ($t_d = \Delta_{eff}$) and exchange time scale (τ_i). For the homogeneity assumption to hold, the mass exchange between compartments should be barrier-limited, which is characterized by $\tau_i << l_r^2/D$ (Moutal et al., 2018) and should also be measured in the slow exchange regime, i.e. $\tau_i << 1/q^2 D_{ex}$ (Meier et al., 2003). These constraints are satisfied for small cell sizes and low membrane permeability (Coatléven et al., 2014; Haddar et al., 2016; Fieremans et al., 2010). Fortuitously, this applies to myelinated axons, hence the widespread applications of the 2CE model in brain white matter dMRI, however, as seen above, extending this model to muscle is not warranted. Analyzing the breakdown of the 2CE model in terms of the above characteristic scales is useful to show not only why such models do not work in muscle, but also to develop some generalized bounds (similar to those done by Moutal et al. (2018)) which should help guide future model development.

The homogenization approximation made in compartmental exchange models is also made in the field of mass transfer (the lumped capacitance approximation). As such, it is useful to draw an analogy with the dimensionless numbers developed in that field, namely the Biot and Fourier numbers. The mass transfer Biot number ($B = \kappa L/D$ where L is the characteristic length scale of the particular homogenized compartment, often the volume to surface area ratio) is the dimensionless ratio of the membrane permeability to diffusivity of the compartment. The Fourier number ($F = t_d D/L^2$) is the ratio of the diffusion distance to the compartment's length scale. When F >> 1, the entire compartment is probed by the diffusing spins leading to the validity of a long time limit approximation. In this case, the accuracy for the 2CE model is determined by the Biot number. For B << 1 (typically B < 0.1), the compartment can be modeled as a single homogeneous domain in terms of mass transfer because the mass transfered through the membrane (associated with signal gradients near the boundary) is small compared with the mass diffused within the compartment. The conditions of large Fourier and small Biot numbers are satisfied for myelinated axons. However, the 2CE model can also be applicable in the short diffusion time limit. In this short time limit of F << 1, rather than being on B, the constraint is on the combination of F and B such that $F \cdot B << 1$ ($F \cdot B = t_d \kappa/L$). This constraint implies that the diffusion distance is much less than the length scale of the compartment, so signal gradients are confined in a thin boundary layer in the vicinity of the membrane resulting in a predominantly homogeneous signal distribution. This criterion is only qualitative as it does not address the magnitude of the signal gradients at the membrane. This regime can be seen in Figure 4a, where the intracellular signal agrees for small cell sizes (F>>1) and also for large cell sizes (F<<1). There is also a limited effect of the permeability in the formulation of this criterion for the homogeneity approximation: κ must be small

enough so that $F \cdot B << 1$.

The above conditions suggest regimes where the key underlying assumption for the 2CE model (the signal in each compartment can be considered homogeneous) is valid, but they do not address the other limitations of the 2CE model in modeling the evolution of the signal in each compartment. At high volume fractions, for example, it is possible that the extracellular compartment satisfies F >> 1 and B << 1, however, this only suggests that the signal in this compartment is homogeneous, not that the 2CE model is appropriate. Kärger-type models also hinge on the assumption that the compartmental diffusion coefficients can be modeled by the Gaussian (long-time limit) solution of the signal in that compartment. This is also true when the model is constructed on the basis of formal homogenization theory (Fieremans et al., 2010; Coatléven et al., 2014). A more appropriate phenomenological approach is to modify the requirement to account for the time-dependence of the ADC, particularly when modeling the intracellular compartment (Stanisz et al., 1997; Karampinos et al., 2009). However, using such an approach for the extracellular space is hampered by a lack of analytical solutions for the tortuous extracellular geometry (Haddar et al., 2016; Li et al., 2014). Some proposals to overcome this obstacle include using numerical, long-time limit solutions, from which the modified ADC is derived based on a tortuosity factor (Nilsson et al., 2010; Fieremans et al., 2010; Li et al., 2014). However, as Figure 4c shows, even when an accurate analytical solution is available, the long-time limit approximation for the extracellular space is not appropriate when $l_d \lesssim l_r$. Accounting for this time dependence of the extracellular compartment's ADC requires solving elliptic partial differential equations (Haddar et al., 2016), which is of debatable advantage compared with directly solving the Bloch-Torrey equation numerically, as done here with the LBM scheme, since the Bloch-Torrey equation is of the same type as the equations proposed in Haddar et al. (2016).

The numerical results presented here suggest that the current 2CE model formulation is in general not suitable for skeletal muscle due to inaccuracies in handling larger cell sizes, high volume fractions, and finite permeability values. However, the introduction of the dimensionless numbers F and B points to the possibility that there might exist possible regimes of applicability for the 2CE model in muscle. Using typical parameters for skeletal myocytes (diameter of 50 microns, diffusion coefficient of 2 $\mu m^2/ms$, membrane permeability of 20 $\mu m/s$, endomysium thickness of 3 μm, and a diffusion time of 50 ms), one finds that the intracellular compartment is characterized by F = 0.04 and $F \cdot B = 0.02$ and the extracellular compartment by F = 11 and B = 0.03. Both compartments satisfy the validity criterion for the two-compartment model approximation, with signal evolution in one compartment in the short time limit while the other is in the long time limit. By combining long and short time limit solutions for the respective compartments it may be possible to refine the two-compartment model to apply to skeletal muscle, however, the 2CE model is not currently formulated in this fashion. A better method for determining the effective diffusion coefficient of the extracellular compartment needs to be developed, as well as an understanding of how

the long and short time limit solutions interact through the exchange term.

dMRI is less developed for skeletal muscle, not only for historical reasons but also because the interpretation of the biological basis of the signal is more complex than neural tissue. Developing an accurate 2CE model for skeletal muscle will aid in interpreting dMRI measurements because of the efficiency with which the 2CE model can be employed in solving the inverse problem. We have compared a two-compartment exchange model (2CE) with a lattice Boltzmann method (LBM) model and demonstrated that, although the 2CE model is accurate for brain tissue, such models are not appropriate for skeletal muscle. The random permeable barrier model, another analytical model of skeletal muscle diffusion, abstracts the extracellular compartment as random barriers (Fieremans et al., 2017). The topology of the extracellular compartment is an important functional element of the hierarchical extracellular matrix (ECM) of muscle, so this simplification reduces the ability to extract realistic microstructural parameters from muscle dMRI measurements. Since the configuration of ECM is intimately related to force transmission (Karampinos et al., 2009; Lieber and Ward, 2013), reduction in structural information will diminish the ability of dMRI to inform micro-mechanical models of skeletal tissue. Both analytical models appear to be lacking in their ability to accurately model the underlying extracellular microstructure which gives rise to diffusion-weighted signal. In order to interpret dMRI measurements quantitatively in relation to the skeletal muscle microstructure (particularly its extracellular structure), we propose reverting to numerical methods, such as Monte Carlo, finite difference, finite element, or LBM to solve the Bloch-Torrey equation on a continuum tissue model.

5. Conclusion

The present numerical study is driven by the need to assess the applicability of the two-compartment exchange (2CE) model for the simulation of the dMRI signal in muscle. A two dimensional composite tissue model consisting of a periodic array of cylindrical cells is considered. The 2CE results are compared with the continuum solution obtained by solving the Bloch-Torrey equation numerically via a hybrid-LBM scheme. This comparison shows that the 2CE model is accurate for small diameter cells with low cell volume fraction and membrane permeability, but it becomes progressively inaccurate as diameter and cell volume fraction increases. A systematic description of the valid domain of the 2CE model is proposed in terms of two dimensionless parameters inspired by the field of mass transfer: the Fourier number (F), defined as the ratio of diffusion distance to cell length scale, and the Biot number (B), the ratio of intercompartment exchange to diffusion flux. The 2CE model is valid for $B << 1$ and $F >> 1$ as well as $F << 1$ and $F \cdot B << 1$. The signal in each compartment is examined separately and the major source of inaccuracy is found to be associated with errors in modeling diffusion in the extracellular space.

6. Acknowledgments

We acknowledge the financial support by NSF (grants CBET-1236451 & CMMI-1437113, and a Graduate Research Fellowship to NMN). Partial support by the R.A. Pritzker chair fund is also acknowledged.

References

Ababneh, Z., Beloeil, H., Berde, C. B., Gambarota, G., Maier, S. E. and Mulkern, R. V. (2005). Biexponential parameterization of diffusion and T2 relaxation decay curves in a rat muscle edema model: decay curve components and water compartments, *Magnetic Resonance in Medicine* **54**(3): 524–531.

Åslund, I. and Topgaard, D. (2009). Determination of the self-diffusion coefficient of intracellular water using PGSE NMR with variable gradient pulse length, *Journal of Magnetic Resonance* **201**(2): 250–254.

Assaf, Y., Blumenfeld-Katzir, T., Yovel, Y. and Basser, P. J. (2008). Axcaliber: a method for measuring axon diameter distribution from diffusion MRI, *Magnetic Resonance in Medicine* **59**(6): 1347–1354.

Babsky, A. M., Topper, S., Zhang, H., Gao, Y., James, J. R., Hekmatyar, S. K. and Bansal, N. (2008). Evaluation of extra- and intracellular apparent diffusion coefficient of sodium in rat skeletal muscle: Effects of prolonged ischemia, *Magnetic Resonance in Medicine* **59**(3): 485–491.

Bates, J., Teh, I., McClymont, D., Kohl, P., Schneider, J. E. and Grau, V. (2017). Monte Carlo simulations of diffusion weighted MRI in myocardium: Validation and sensitivity analysis, *IEEE Transactions on Medical Imaging* **36**(6): 1316–1325.

Beaulieu, C. (2002). The basis of anisotropic water diffusion in the nervous system – a technical review, *NMR in Biomedicine* **15**(7-8): 435–455.

Beltrachini, L., Taylor, Z. A. and Frangi, A. F. (2015). A parametric finite element solution of the generalised Bloch–Torrey equation for arbitrary domains, *Journal of Magnetic Resonance* **259**: 126–134.

Berry, D. B., Regner, B., Galinsky, V., Ward, S. R. and Frank, L. R. (2018). Relationships between tissue microstructure and the diffusion tensor in simulated skeletal muscle, *Magnetic Resonance in Medicine* **80**(1): 317–329.

Bolsterlee, B., D'Souza, A., Gandevia, S. C. and Herbert, R. D. (2017). How does passive lengthening change the architecture of the human medial gastrocnemius muscle?, *Journal of Applied Physiology* **122**(4): 727–738.

Boonyarom, O. and Inui, K. (2006). Atrophy and hypertrophy of skeletal muscles: structural and functional aspects, *Acta Physiologica* **188**(2): 77–89.

Callaghan, P. T. (1997). A simple matrix formalism for spin echo analysis of restricted diffusion under generalized gradient waveforms, *Journal of Magnetic Resonance* **129**(1): 74–84.

Chen, S. and Doolen, G. D. (1998). Lattice Boltzmann method for fluid flows, *Annual Review of Fluid Mechanics* **30**(1): 329–364.

Coatléven, J., Haddar, H. and Li, J.-R. (2014). A macroscopic model including membrane exchange for diffusion MRI, *SIAM Journal on Applied Mathematics* **74**(2): 516–546.

Codd, S. L. and Callaghan, P. T. (1999). Spin echo analysis of restricted diffusion under generalized gradient waveforms: planar, cylindrical, and spherical pores with wall relaxivity, *Journal of Magnetic Resonance* **137**(2): 358–372.

Fieremans, E., Lemberskiy, G., Veraart, J., Sigmund, E. E., Gyftopoulos, S. and Novikov, D. S. (2017). In vivo measurement of membrane permeability and myofiber size in human muscle using time-dependent diffusion tensor imaging and the random permeable barrier model, *NMR in Biomedicine* **30**(3).

Fieremans, E., Novikov, D. S., Jensen, J. H. and Helpern, J. A. (2010). Monte Carlo study of a two-compartment exchange model of diffusion, *NMR in Biomedicine* **23**(7): 711–724.

Filli, L., Kenkel, D., Wurnig, M. C. and Boss, A. (2016). Diffusional kurtosis MRI of the lower leg: changes caused by passive muscle elongation and shortening, *NMR in Biomedicine* **29**(6): 767–775.

Froeling, M., Oudeman, J., Strijkers, G. J., Maas, M., Drost, M. R., Nicolay, K. and Nederveen, A. J. (2015). Muscle changes detected with diffusion-tensor imaging after long-distance running, *Radiology* **274**(2): 548–562.

Froeling, M., Strijkers, G. J., Nederveen, A. J., Chamuleau, S. A. and Luijten, P. R. (2014). Diffusion tensor MRI of the heart - in vivo imaging of myocardial fiber architecture, *Current Cardiovascular Imaging Reports* **7**(7): 1–11.

Galban, C. J., Maderwald, S., Uffmann, K., de Greiff, A. and Ladd, M. E. (2004). Diffusive sensitivity to muscle architecture: a magnetic resonance diffusion tensor imaging study of the human calf, *European Journal of Applied Physiology* **93**(3): 253–262.

Galbán, C. J., Maderwald, S., Uffmann, K. and Ladd, M. E. (2005). A diffusion tensor imaging analysis of gender differences in water diffusivity within human skeletal muscle, *NMR in Biomedicine* **18**(8): 489–498.

Grebenkov, D. S. (2010). Pulsed-gradient spin-echo monitoring of restricted diffusion in multilayered structures, *Journal of Magnetic Resonance* **205**(2): 181–195.

Haddar, H., Li, J.-R. and Schiavi, S. (2016). A macroscopic model for the diffusion MRI signal accounting for time-dependent diffusivity, *SIAM Journal on Applied Mathematics* **76**(3): 930–949.

Hagslätt, H., Jönsson, B., Nydén, M. and Söderman, O. (2003). Predictions of pulsed field gradient NMR echo-decays for molecules diffusing in various restrictive geometries. simulations of diffusion propagators based on a finite element method, *Journal of Magnetic Resonance* **161**(2): 138–147.

Häkkinen, K., Newton, R. U., Gordon, S. E., McCormick, M., Volek, J. S., Nindl, B. C., Gotshalk, L. A., Campbell, W. W., Evans, W. J., Häkkinen, A. et al. (1998). Changes in muscle morphology, electromyographic activity, and force production characteristics during progressive strength training in young and older men, *The Journals of Gerontology Series A: Biological Sciences and Medical Sciences* **53**(6): B415–B423.

Hall, M. G. and Alexander, D. C. (2009). Convergence and parameter choice for Monte-Carlo simulations of diffusion MRI, *IEEE Transactions on Medical Imaging* **28**(9): 1354–1364.

Hall, M. G. and Clark, C. A. (2017). Diffusion in hierarchical systems: A simulation study in models of healthy and diseased muscle tissue, *Magnetic Resonance in Medicine* **78**(3): 1187–1198.

Harkins, K. D., Galons, J.-P., Secomb, T. W. and Trouard, T. P. (2009). Assessment of the effects of cellular tissue properties on ADC measurements by numerical simulation of water diffusion, *Magnetic Resonance in Medicine* **62**(6): 1414–1422.

Heemskerk, A. M. and Damon, B. M. (2007). Diffusion tensor MRI assessment of skeletal muscle architecture, *Current medical imaging reviews* **3**(3): 152–160.

Heemskerk, A. M., Sinha, T. K., Wilson, K. J., Ding, Z. and Damon, B. M. (2010). Repeatability of DTI-based skeletal muscle fiber tracking, *NMR in Biomedicine* **23**(3): 294–303.

Helmer, K., Seland, J., Henninger, N. and Sotak, C. (2006). Separation of the intra- and extracellular apparent diffusion coefficients (ADC) of water in rat skeletal muscle using spectroscopic MEMRI, ISMRM.

Hwang, S. N., Chin, C.-L., Wehrli, F. W. and Hackney, D. B. (2003). An image-based finite difference model for simulating restricted diffusion, *Magnetic Resonance in Medicine* **50**(2): 373–382.

Jelescu, I. O. and Budde, M. D. (2017). Design and validation of diffusion MRI models of white matter, *Frontiers in physics* **5**: 61.

Jiang, X., Li, H., Xie, J., Zhao, P., Gore, J. C. and Xu, J. (2016). Quantification of cell size using temporal diffusion spectroscopy, *Magnetic Resonance in Medicine* **75**(3): 1076–1085.

Karampinos, D. C., King, K. F., Sutton, B. P. and Georgiadis, J. G. (2007). In vivo study of cross-sectional skeletal muscle fiber asymmetry with diffusion-weighted MRI, *Annual International Conference of the IEEE Engineering in Medicine and Biology - Proceedings*, IEEE, pp. 327–330.

Karampinos, D. C., King, K. F., Sutton, B. P. and Georgiadis, J. G. (2009). Myofiber ellipticity as an explanation for transverse asymmetry of skeletal muscle diffusion MRI in vivo signal, *Annals of Biomedical Engineering* **37**(12): 2532–2546.

Kärger, J. (1988). Principles and applications of self-diffusion measurements by nuclear magnetic resonance, *Adv Magn Reson* **12**: 1–89.

Kim, S., Chi-Fishman, G., Barnett, A. S. and Pierpaoli, C. (2005). Dependence on diffusion time of apparent diffusion tensor of ex vivo calf tongue and heart, *Magnetic Resonance in Medicine* **54**(6): 1387–1396.

Kinsey, S. T., Locke, B. R., Penke, B. and Moerland, T. S. (1999). Diffusional anisotropy is induced by subcellular barriers in skeletal muscle, *NMR in Biomedicine* **12**(1): 1–7.

Laghi, L., Venturi, L., Dellarosa, N. and Petracci, M. (2017). Water diffusion to assess meat microstructure, *Food Chemistry* **236**: 15–20.

Landis, C. S., Li, X., Telang, F. W., Molina, P. E., Palyka, I. and Vetek, G. (1999). Equilibrium transcytolemmal water-exchange kinetics in skeletal muscle in vivo, *Magnetic Resonance in Medicine* **42**(3): 467–478.

Lansdown, D. A., Ding, Z., Wadington, M., Hornberger, J. L. and Damon, B. M. (2007). Quantitative diffusion tensor MRI-based fiber tracking of human skeletal muscle, *Journal of Applied Physiology* **103**(2): 673–681.

Lee, C.-Y., Bennett, K. M. and Debbins, J. P. (2013). Sensitivities of statistical distribution model and diffusion kurtosis model in varying microstructural environments: a Monte Carlo study, *Journal of Magnetic Resonance* **230**: 19–26.

Li, J.-R., Nguyen, H. T., Van Nguyen, D., Haddar, H., Coatléven, J. and Le Bihan, D. (2014). Numerical study of a macroscopic finite pulse model of the diffusion MRI signal, *Journal of Magnetic Resonance* **248**: 54–65.

Li, L., Mei, R. and Klausner, J. F. (2013). Boundary conditions for thermal lattice Boltzmann equation method, *Journal of Computational Physics* **237**: 366–395.

Lieber, R. L. and Ward, S. R. (2013). Cellular mechanisms of tissue fibrosis. 4. structural and functional consequences of skeletal muscle fibrosis, *American Journal of Physiology-Cell Physiology* **305**(3): C241–C252.

McConnell, H. M. (1958). Reaction rates by nuclear magnetic resonance, *The Journal of Chemical Physics* **28**(3): 430–431.

Meier, C., Dreher, W. and Leibfritz, D. (2003). Diffusion in compartmental systems. i. a comparison of an analytical model with simulations, *Magnetic Resonance in Medicine* **50**(3): 500–509.

Mekkaoui, C., Reese, T. G., Jackowski, M. P., Bhat, H. and Sosnovik, D. E. (2017). Diffusion MRI in the heart, *NMR in Biomedicine* **30**(3): e3426.

Morvan, D. (1995). In vivo measurement of diffusion and pseudo-diffusion in skeletal muscle at rest and after exercise, *Magnetic Resonance Imaging* **13**(2): 193–199.

Moutal, N., Nilsson, M., Topgaard, D. and Grebenkov, D. (2018). The Kärger vs bi-exponential model: Theoretical insights and experimental validations, *Journal of Magnetic Resonance* **296**: 72–78.

Naughton, N. M., Tennyson, C. G. and Georgiadis, J. G. (submitted 2019). Lattice Boltzmann method for simulation of diffusion magnetic resonance imaging physics in heterogeneous tissue models, *Journal of Computational Physics* . preprint available at https://git.io/fhodg.

Nguyen, H. T., Grebenkov, D., Van Nguyen, D., Poupon, C., Le Bihan, D. and Li, J.-R. (2015). Parameter estimation using macroscopic diffusion MRI signal models, *Physics in Medicine and Biology* **60**(8): 3389.

Nilsson, M., Alerstam, E., Wirestam, R., Sta, F., Brockstedt, S., Lätt, J. et al. (2010). Evaluating the accuracy and precision of a two-compartment Kärger model using Monte Carlo simulations, *Journal of Magnetic Resonance* **206**(1): 59–67.

Novikov, D. S., Fieremans, E., Jensen, J. H. and Helpern, J. A. (2011). Random walks with barriers, *Nature Physics* **7**(6): 508–514.

Oudeman, J., Nederveen, A. J., Strijkers, G. J., Maas, M., Luijten, P. R. and Froeling, M. (2016). Techniques and applications of skeletal muscle diffusion tensor imaging: A review, *Journal of Magnetic Resonance Imaging* **43**(4): 773–788.

Perrins, W., McKenzie, D. and McPhedran, R. (1979). Transport properties of regular arrays of cylinders, *Proceedings of the Royal Society of London A: Mathematical, Physical and Engineering Sciences* **369**(1737): 207–225.

Polgar, J., Johnson, M., Weightman, D. and Appleton, D. (1973). Data on fibre size in thirty-six human muscles: An autopsy study, *Journal of the Neurological Sciences* **19**(3): 307–318.

Porcari, P., Hall, M. G., Clark, C. A., Greally, E., Straub, V. and Blamire, A. M. (2018). The effects of ageing on mouse muscle microstructure: a comparative study of time-dependent diffusion MRI and histological assessment, *NMR in Biomedicine* **31**(3): e3881.

Purslow, P. P. (2002). The structure and functional significance of variations in the connective tissue within muscle, *Comparative Biochemistry and Physiology Part A: Molecular & Integrative Physiology* **133**(4): 947–966.

Russell, G., Harkins, K. D., Secomb, T. W., Galons, J.-P. and Trouard, T. P. (2012). A finite difference method with periodic boundary conditions for simulations of diffusion-weighted magnetic resonance experiments in tissue, *Physics in Medicine and Biology* **57**(4): N35.

Saab, G., Thompson, R. T. and Marsh, G. D. (1999). Multicomponent T2 relaxation of in vivo skeletal muscle, *Magnetic Resonance in Medicine* **42**(1): 150–157.

Saotome, T., Sekino, M., Eto, F. and Ueno, S. (2006). Evaluation of diffusional anisotropy and microscopic structure in skeletal muscles using magnetic resonance, *Magnetic Resonance Imaging* **24**(1): 19–25.

Scheel, M., von Roth, P., Winkler, T., Arampatzis, A., Prokscha, T., Hamm, B. and Diederichs, G. (2013). Fiber type characterization in skeletal muscle by diffusion tensor imaging, *NMR in Biomedicine* **26**(10): 1220–1224.

Seland, J. G., Bruvold, M., Anthonsen, H., Brurok, H., Nordhøy, W., Jynge, P. and Krane, J. (2005). Determination of water compartments in rat myocardium using combined D–T1 and T1–T2 experiments, *Magnetic Resonance Imaging* **23**(2): 353–354.

Sen, P. N. and Basser, P. J. (2005). A model for diffusion in white matter in the brain, *Biophysical Journal* **89**(5): 2927–2938.

Sigmund, E. E., Novikov, D. S., Sui, D., Ukpebor, O., Baete, S., Babb, J. S., Liu, K., Feiweier, T., Kwon, J., Mcgorty, K., Bencardino, J. and Fieremans, E. (2014). Time-dependent diffusion in skeletal muscle with the random permeable barrier model (RPBM): Application to normal controls and chronic exertional compartment syndrome patients, *NMR in Biomedicine* **27**(5): 519–528.

Silva, M. D., Helmer, K. G., Lee, J.-H., Han, S. S., Springer, C. S. and Sotak, C. H. (2002). Deconvolution of compartmental water diffusion coefficients in yeast-cell suspensions using combined T1 and diffusion measurements, *Journal of Magnetic Resonance* **156**(1): 52–63.

Söderman, O. and Jönsson, B. (1995). Restricted diffusion in cylindrical geometry, *Journal of Magnetic Resonance, Series A* **117**(1): 94–97.

Stanisz, G. J., Li, J. G., Wright, G. A. and Henkelman, R. M. (1998). Water dynamics in human blood via combined measurements of T2 relaxation and diffusion in the presence of gadolinium, *Magnetic Resonance in Medicine* **39**(2): 223–233.

Stanisz, G. J., Wright, G. A., Henkelman, R. M. and Szafer, A. (1997). An analytical model of restricted diffusion in bovine optic nerve, *Magnetic Resonance in Medicine* **37**(1): 103–111.

Stejskal, E. O. and Tanner, J. E. (1965). Spin diffusion measurements: spin echoes in the presence of a time-dependent field gradient, *The Journal of Chemical Physics* **42**(1): 288–292.

Szafer, A., Zhong, J. and Gore, J. C. (1995). Theoretical model for water diffusion in tissues, *Magnetic Resonance in Medicine* **33**(5): 697–712.

Tanner, J. E. (1978). Transient diffusion in a system partitioned by permeable barriers. application to NMR measurements with a pulsed field gradient, *The Journal of Chemical Physics* **69**(4): 1748–1754.

Tanner, J. E. and Stejskal, E. O. (1968). Restricted self-diffusion of protons in colloidal systems by the pulsed-gradient, spin-echo method, *The Journal of Chemical Physics* **49**(4): 1768–1777.

Torrey, H. C. (1956). Bloch equations with diffusion terms, *Physical Review* **104**(3): 563.

Van Nguyen, D., Li, J.-R., Grebenkov, D. and Le Bihan, D. (2014). A finite elements method to solve the Bloch–Torrey equation applied to diffusion magnetic resonance imaging, *Journal of Computational Physics* **263**: 283–302.

Xu, J., Does, M. D. and Gore, J. C. (2007). Numerical study of water diffusion in biological tissues using an improved finite difference method, *Physics in Medicine and Biology* **52**(7): N111.